

Article

Phase Transformation Behavior of a β -Solidifying γ -TiAl-Based Alloy from Different Phase Regions with Various Cooling Methods

Xiaobing Li ¹, Hao Xu ^{1,2}, Weiwei Xing ¹, Bo Chen ¹, Yingche Ma ^{1,*}  and Kui Liu ^{1,*}

¹ Institute of Metal Research, Chinese Academy of Sciences, Shenyang 110016, China; xbli@imr.ac.cn (X.L.); hxu12s@imr.ac.cn (H.X.); wwxing@imr.ac.cn (W.X.); bchen@imr.ac.cn (B.C.)

² University of Chinese Academy of Sciences, Beijing 100049, China

* Correspondence: ycma@imr.ac.cn (Y.M.); kliu@imr.ac.cn (K.L.);
Tel.: +86-024-2397-1986 (Y.M. & K.L.); Fax: +86-024-2389-1320 (Y.M. & K.L.)

Received: 29 August 2018; Accepted: 10 September 2018; Published: 17 September 2018



Abstract: The phase transformation behavior of Ti-42Al-5Mn (at.%) alloy from different phase regions with various cooling rates was investigated based on electron probe micro analyzer-backscattered electrons (EPMA-BSE). It is shown that $\beta \rightarrow \alpha_2'$ takes place when this alloy is cooled at a high rate, such as water quenching (WQ), oil cooling (OC), from β single phase. With the decreasing cooling rate to air cooling (AC), $\beta \rightarrow \alpha_2'$ is restrained and $\beta \rightarrow \gamma$ is promoted by forming γ platelets. The room-temperature microstructure is $\beta_o + \alpha_2$ when alloy cooled (WQ and OC) from ($\beta + \alpha$) dual-phase. However, under AC, $\beta \rightarrow \gamma$ occurs and γ platelets form. It should be noted that $\alpha_2 \rightarrow \gamma$ happens when this alloy cooled from 1180 °C ($>T_{eut}$) by OC and AC, forming an incomplete lamellae (α_2/γ) structure in the α_2 phase. However, when the alloy cooled from 1100 °C ($<T_{eut}$), $\alpha_2/\gamma \rightarrow \beta_{o,sec}$ occurs and complete lamellae generates in α_2 phase.

Keywords: titanium aluminides; β -solidifying; phase transformation; microstructural evolution

1. Introduction

In general, Ti and Ti alloys are quite attractive for aerospace, medical, and industrial applications [1–4], of which gamma-titanium aluminide (γ -TiAl) has been considered as one of the topmost candidates for high-temperature structural material due to its low density and high specific modulus and strength [5–9]. However, the intricate processing behavior, particularly the poor ductility and the low hot workability appears to be the main obstacle for a wide industrial application of γ -TiAl alloys [9]. In 1997, β -solidifying γ -TiAl alloys (via β -phase solidification) were proposed by Naka [10], also called beta solidified gammalloys (BSG) by Kim in 2018 [11], arousing increasing attention due to their excellent workability and the appropriate solidification process without any peritectic segregation [12]. These BSG alloys usually have one or more β stabilizing elements, such as Mo, Cr, Mn, V, Nb and a lower Al concentration (42–44%) when compared to conventional gammalloys (CG) [11], which finally results in their solidification pathway going through the single β -phase region.

As for the CG alloys, typically four types of microstructures can be obtained by heat treatment around the gamma dissolution temperature ($T_{\gamma solv}$), namely fully lamellar (FL), nearly lamellar (NL), duplex (DP) and near gamma (NG) [13,14]. The solidification procedure from the liquid to the stable solid state for the CG alloys can be given as $L \rightarrow L + \beta \rightarrow (\beta + \alpha)$ or $(L + \alpha) \rightarrow \alpha \rightarrow \alpha + \gamma \rightarrow \alpha_2 + \gamma$. In the case of BSG alloys, since they contain a sufficient amount of β -stabilizing elements, the solidification pathway appears to be more complicated, and the typical structures of CG alloys are also no longer applicable. Clemens et al. [15,16] defined three types of structures for Ti-43.5Al-4Nb-1Mo-0.1B (TNM)

alloy (BSG), including NL + β_1 , NL + β_2 , and NL + γ . The three microstructure consist of $\alpha_2/\gamma + \beta_o + \gamma$, but there are significant differences in their morphology. From the aspect of the γ phase morphology, the γ phase in the first two kinds of structure is platelet, and the γ phase in the latter structure is block. Compared with NL + β_1 and NL + β_2 , the difference between the two microstructures is that there are very few $\beta_{o,sec}$ and γ phases around the colony boundary for NL + β_1 , while there are plenty of $\beta_{o,sec}$ and γ phases for NL + β_2 .

Ti-42Al-5Mn, developed by Tetsui et al. in 2002 [17], is a typical BSG alloy, and it has the advantage of low cost and great workability, and seems to be a promising material for automotive industrial applications. Since then, Tetsui et al. reported some studies on this alloy from 2002 to 2013 [18–20], but their investigations were still limited to smelting and forging. Our team has also conducted more in-depth research on Ti-42Al-5Mn in recent years. Our previous research confirmed its solidification pathway from the liquid to room temperature as the following: liquid \rightarrow liquid + $\beta \rightarrow \beta \rightarrow \beta + \alpha \rightarrow \beta + \alpha + \gamma \rightarrow \beta_o + \alpha_2 + \gamma \rightarrow \beta_o + \gamma + \alpha_2/\gamma \rightarrow \beta_o + \gamma + \alpha_2/\gamma + \beta_{o,sec}$, with the $T_\beta = 1311$ °C, $T_{\gamma solv} = 1231$ °C, $T_{\beta \rightarrow \beta_o/\alpha \rightarrow \alpha_2} = 1168$ °C, $T_{eut} = 1132$ °C and $T_{\alpha_2/\gamma \rightarrow \beta_{o,sec}} \approx 1120$ °C [21]. On this basis, the continuous cooling transformation curve (CCT) of the forged alloy was examined and a CCT diagram of the alloy was established [22]. It has been found that five kinds of phase transformation exist during continuous cooling from 1300 °C (forging temperature) with the cooling rates of 0.1 °C/s, 0.5 °C/s, 2 °C/s, 10 °C/s, 50 °C/s, and 200 °C/s, including $\beta \rightarrow \alpha$, $\beta \rightarrow \gamma$, $\beta \rightarrow \beta_o/\alpha \rightarrow \alpha_2$, $\alpha_2 \rightarrow \alpha_2/\gamma$ and $\alpha_2/\gamma \rightarrow \beta_{o,sec}$. Despite this, the study of the alloy is still at an initial stage; the corresponding microstructure evolution and phase transformation are not well understood. In order to exert the advantages of the alloy, it is overwhelmingly indispensable to grasp their phase transformation behavior.

In the present study, the phase transformation behavior of as-casted Ti-42Al-5Mn alloy from different phase regions (β , $\alpha + \beta$, $\alpha + \beta + \gamma$) with various cooling rate was further investigated. The work aimed to clarify the phase transition characteristics of Ti-42Al-5Mn in order to provide fundamental data, knowledge and information (DKI) for BSG alloy development.

2. Experimental Methods

Ti-42Al-5Mn (designated 42Al-5Mn) (at.%) as-cast ingot, with the dimension of $\Phi 120$ mm \times 400 mm, was prepared by the Institute of Metal Research (IMR) (Shenyang, China) improved vacuum induction melting (VIM) and vacuum arc remelting (VAR) using titanium sponge (99.9 wt.%), pure aluminum (99.9 wt.%), and purified manganese (99 wt.%).

The samples with size of $\Phi 8$ mm \times 8 mm were cut along the edge of the foot section of the as-cast ingot. Subsequently, each sample was put into a separate sealing tube filled with argon atmosphere to avoid oxidation, and the sealing tube was then placed in the muffle furnace. In order to ensure the consistency of each experiment, the samples were first heated to 1340 °C to ensure the α_2/γ lamellae and γ grain could be completely dissolved into the β phase. After holding for 30 min, samples were cooled by water quenching (WQ), oil cooling (OC), and air cooling (AC), and the decreasing ordering in cooling speed was WQ, OC, AC [23]. The other specimens were then furnace cooled (FC, valued about 5 °C \cdot min⁻¹ [24]) to the target temperatures of 1260 °C ($\alpha + \beta$), 1180 °C ($\alpha + \beta + \gamma$, close to T_{eut}), and 1100 °C ($\alpha + \beta + \gamma$). After holding for 30 min, these samples were also cooled with the WQ, OC, and AC methods, as illustrated in Figure 1. The microstructures of the specimens were characterized by electron probe micro analyzer (EPMA, JXA-8230, Northeastern University, Shenyang, China) with back scattered electron (BSE) and wave dispersive spectroscopy (WDS) mode.

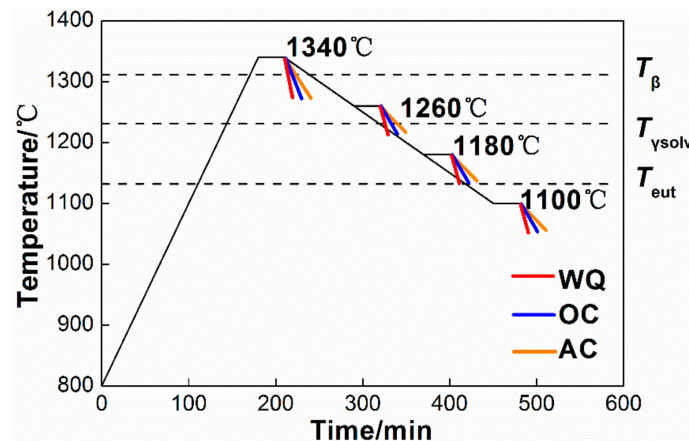


Figure 1. Schematic diagram of continuous cooling transformation experiments.

3. Results

3.1. Microstructure Cooled from 1340 °C

Figure 2 shows the microstructure characteristics of the samples subjected to 1340 °C with different cooling methods. In this paper, β_0 (ordered body-centered cubic (bcc) B2 structure) and α_2 (ordered hexagonal $D0_{19}$ structure) are used to describe the room-temperature phase composition. The reason is that the disorder–order phase transformation shows the least sensitivity to the cooling rate in γ -TiAl alloy, namely a high cooling rate could not suppress the nucleation for the transformation [25].

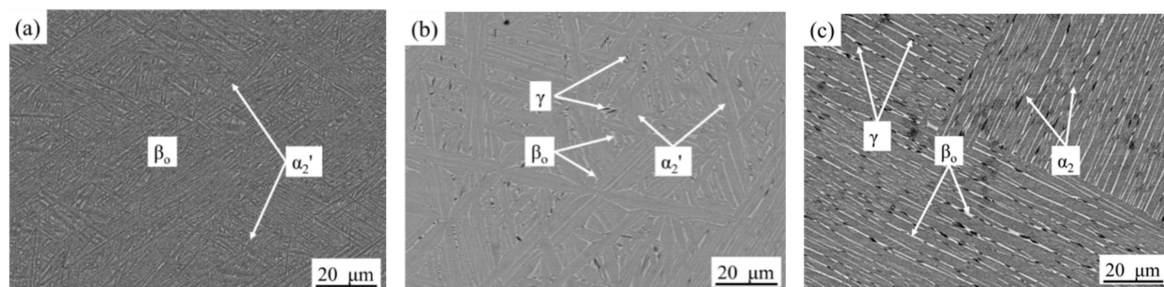


Figure 2. Electron probe micro analyzer (EPMA) results of the samples subjected to (a) 1340 °C/30 min/WQ; (b) 1340 °C/30 min/OC; (c) 1340 °C/30 min/AC. WQ: water quenching; OC: oil cooling; AC: air cooling.

Based on our previous research [21], there should be only pure β phase at 1340 °C since the Ti-42Al-5Mn is in the β single-phase region. However, from Figure 2a, some needlelike martensitic structures, namely α_2' [26] was observed in the above WQ microstructures. As described in reference. [22], the martensitic phase is considered to be the decomposition of β phase by $\beta \rightarrow \alpha_2'$. Moreover, upon quenching from the single β -phase field region a martensitic transformation was reported in “high- β ” bearing γ -TiAl based alloys, such as TiAl-Mo [26], TiAl-V [27] or TiAl-Nb-Hf [28].

When cooled with the OC method (Figure 2b), the martensitic phase also existed. This means that the $\beta \rightarrow \alpha_2'$ cannot be restrained even though the cooling rate decreases to OC. It can also be seen that the size of α_2' is obviously coarsened due to the relatively lower cooling rate than WQ. Besides, in this situation, some fine γ (ordered face-centered tetragonal $L1_0$ structure) phase named γ -platelets (γ_p) [29] are formed within the β_0 phase, which is the decomposition of the β phase by $\beta \rightarrow \gamma$.

With the cooling rate decreasing to AC (Figure 2c), it can be found that the needlelike martensitic structure disappeared, which suggests that the $\beta \rightarrow \alpha_2'$ is completely restrained at this cooling rate. The β_0 phase is mainly distributed in parallel strips which are quite different from the above samples.

The α_2 phase, defined as the supersaturated α_2 -grain [30], was found between the parallel lines. It should be mentioned that the nucleated γ phase from β_0 was also very fine, which is similar to the OC sample.

3.2. Microstructure Cooled from 1260 °C

Figure 3 presents the microstructure characteristics of the samples subjected to 1260 °C with different cooling methods. As can be seen in Figure 3a, in comparison with Figure 2a, plenty of supersaturated α_2 -grains are precipitated from the single β phase when the sample was cooled from 1340 °C to 1260 °C by furnace cooling. Both the WQ and OC samples consisted of β_0 and α_2 , and no martensitic α_2' phase was detected. This indicates that the $\beta \rightarrow \alpha_2'$ transformation was not only affected by the cooling rate but also influenced by the temperature before cooling.

When it cooled with the AC method (Figure 3c), the microstructure consisted of β_0 , α_2 and γ phases. Lots of fine γ_p were nucleated from the β phase, and the γ phase grew in a staggered manner in the β phase, not parallel, as in Figure 2c.

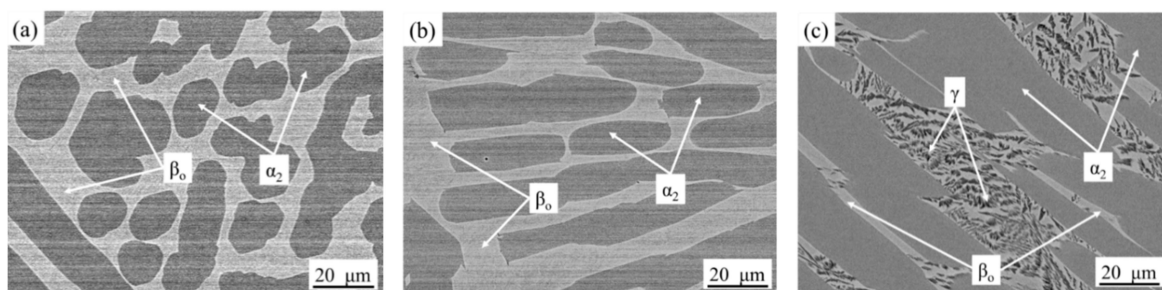


Figure 3. EPMA results of the samples subjected to (a) 1340 °C/30 min/FC to 1260 °C/30 min/WQ; (b) 1340 °C/30 min/FC to 1260 °C/30 min/OC; (c) 1340 °C/30 min/FC to 1260 °C/30 min/AC.

3.3. Microstructure Cooled from 1180 °C

Figure 4 shows the microstructure characteristics of the samples subjected to 1180 °C with different cooling methods. As can be seen in Figure 4a, in comparison with Figure 3a, plenty of globular γ_g grains named γ_g [29] with a median size of 15 μm were nucleated from the β phase. In the α_2 region, a few dispersive γ laths named γ_1 also formed.

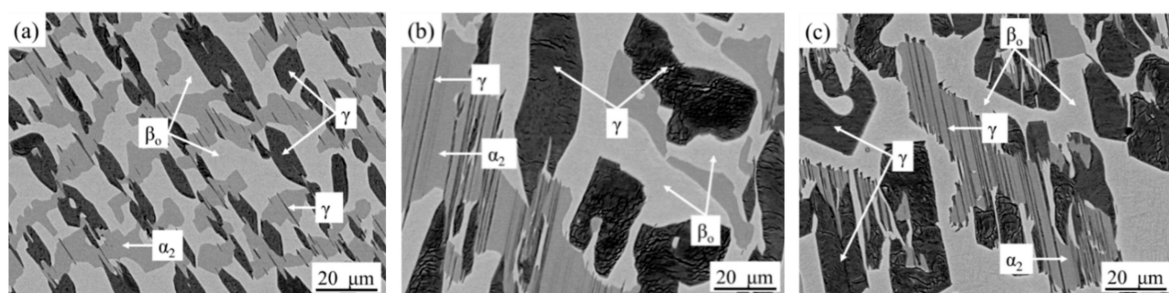


Figure 4. EPMA results of the samples subjected to (a) 1340 °C/30 min/FC to 1180 °C/30 min/WQ; (b) 1340 °C/30 min/FC to 1180 °C/30 min/OC; (c) 1340 °C/30 min/FC to 1180 °C/30 min/AC.

With decreasing cooling rates to OC and AC, the sizes of the γ_g and β_0 phases were all intensively increased to a median size of 40 μm . Moreover, the amount of γ_1 phase in the supersaturated α_2 -grains increased as well. The incomplete α_2/γ lamellae called $(\alpha + \gamma)$ still formed for these three samples, which might be due to the 1180 °C being relatively higher than the T_{eut} (~1140 °C) [21].

3.4. Microstructure Cooled from 1100 °C

Figure 5 shows the microstructure characteristics of the samples subjected to 1100 °C with different cooling methods. As can be seen in Figure 5a, in comparison with Figure 4a, the complete α_2/γ lamellae formed. It should be mentioned that some fine $\beta_{o,sec}$ phases were also nucleated in the lamellae due to the 1100 °C in the temperature range of the $\alpha_2/\gamma \rightarrow \beta_{o,sec}$ transformation. When the cooling rates decreased to OC and AC (Figure 5b,c), the amount of $\beta_{o,sec}$ phases increased. The lamellar spacing and γ grain size also significantly increased with the decreasing cooling rate.

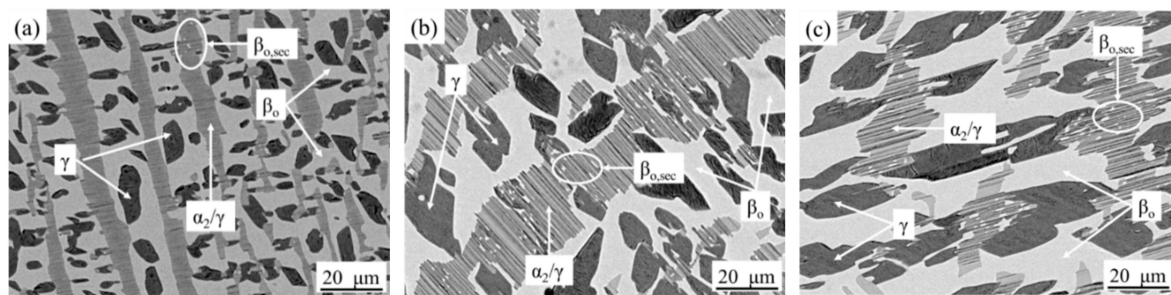


Figure 5. EPMA results of the samples subjected to (a) 1340 °C/30 min/FC to 1100 °C/30 min/WQ; (b) 1340 °C/30 min/FC to 1100 °C/30 min/OC; (c) 1340 °C/30 min/FC to 1100 °C/30 min/AC.

4. Discussion

As stated above, the phase transformation behavior of the Ti-42Al-5Mn alloy from different phase regions with various cooling rate was obtained, as shown in Table 1. It can be seen that the influence of the temperature and cooling rate on the phase transformation and microstructure of this alloy at room temperature was very significant. For the same phase region, with the decrease of the cooling rate, the microstructure of the sample coarsened, and the types of phase transitions increased. This was mainly due to the greater time for the lower cooling rate, which favors more phase transitions.

Table 1. Phase transformation behavior of Ti-42Al-5Mn from different phase regions with various cooling rates.

Temperature/°C	Phase Region [21]	Phase Transformation		
		WQ	OC	AC
1340	β	$\beta \rightarrow \alpha'_2$	$\beta \rightarrow \alpha'_2$	$\beta \rightarrow \alpha, \beta \rightarrow \gamma$
1260	$\beta + \alpha$	/	/	$\beta \rightarrow \alpha, \beta \rightarrow \gamma$
1180	$\beta + \alpha + \gamma$	$\alpha \rightarrow \alpha + \gamma$	$\alpha \rightarrow \alpha + \gamma$	$\alpha \rightarrow \alpha + \gamma$
1100	$\beta + \alpha + \gamma$	$\alpha \rightarrow \alpha_2/\gamma, \alpha/\gamma \rightarrow \beta_{o,sec}$	$\alpha \rightarrow \alpha_2/\gamma, \alpha/\gamma \rightarrow \beta_{o,sec}$	$\alpha \rightarrow \alpha_2/\gamma, \alpha/\gamma \rightarrow \beta_{o,sec}$

It should be mentioned that the γ morphology at room temperature was also closely related to the temperature and cooling rates. Table 2 shows the corresponding relationship between temperature, cooling rate and γ' morphology. As can be seen from this table, three types of γ' morphology can be identified as stated in Section 3, including γ grain or globular (γ_g), γ platelet (γ_p), and γ lath (γ_l), which are illustrated in Figure 6. The γ_g with block morphology, was directly nucleated from the β phase. It was found that when the holding temperature was below $T_{\gamma_{solV}}$, the γ_g could be obtained under the present cooling methods, such as WQ, OC and AC. In the case of γ_p , it was also directly formed in the β phase. However, for this structure, the sample only cooled by AC could be obtained when the holding temperature was above $T_{\gamma_{solV}}$. These fine γ_p phases are usually dispersed in the β region. The third one is γ_l , which was precipitated from the α_2/γ lamellae, and its formation condition was similar to γ_g , i.e., the γ_l phase was almost accompanied by the formation of the γ_g phase. It was ascertained that the treating temperature below $T_{\gamma_{solV}}$ can promote the formation of γ_g and γ_l , and inhibit the appearance of γ_p . Whereas, the temperature above $T_{\gamma_{solV}}$ can restrain the nucleation of γ_g and γ_l ,

and when combined with a relative low cooling rate, for example, the AC method, it will promote the appearance of γ_p .

Although the γ_g and γ_l are all nucleated from the β phase, the size was different between these two phases. It can be seen from Figures 2–5, that the size of γ_g was significantly larger than that of γ_p , which might be the result of their different precipitation conditions. In this study, the fine γ_p is often formed when cooled from a temperature that does not contain the γ phase region, such as the β or ($\beta + \alpha$) phase region. In this situation, the γ_p is precipitated from the β phase during the continuous cooling with a relatively slow cooling rate. Such a phase would have a smaller size compared to the γ_g . However, once the temperature is lowered to the phase region including the γ phase, such as the ($\beta + \alpha + \gamma$) phase region, the pre-precipitated γ phase furnace cooling from 1340 °C to the ($\beta + \alpha + \gamma$) phase region would be further coarsened during the following cooling to form the γ_g . Moreover, it can be also noted that the size of γ_g would be obviously coarsened with a further decrease of the cooling rate. Hence, it is suggested that γ_g and γ_l can be clarified into the same phase, but the grain size between them is different due to their different precipitation behavior.

Table 2. Corresponding relationship between temperature, cooling rate and γ' morphology.

Temperature/°C	1340			1260			1180			1100		
Cooling method	WQ	OC	AC									
γ_g	×	×	×	×	×	×	✓	✓	✓	✓	✓	✓
γ_p	×	×	✓	×	×	✓	×	×	×	×	×	×
γ_l	×	×	×	×	×	×	✓	✓	✓	✓	✓	✓

Note: “×” is not found; “✓” is found.

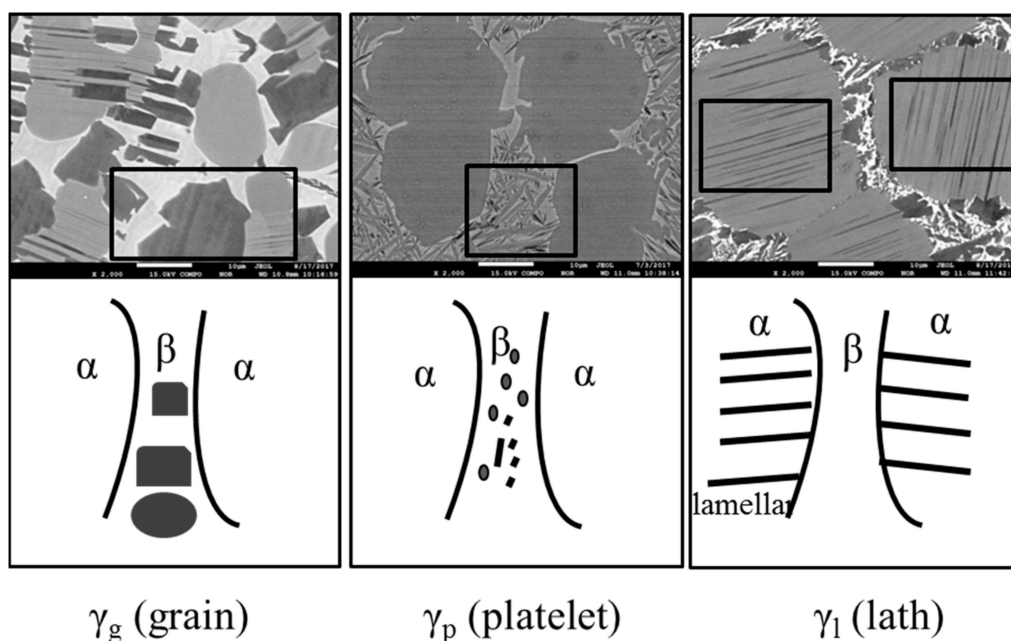


Figure 6. The typical morphology of γ phase in this study.

In fact, the different sizes of γ at the α_2/γ colony boundary have a significant effect on the properties of the γ -TiAl alloy. For the globular γ phase (γ_g), Mayer et al. [15] suggested that the γ_g at the α_2/γ colony boundary is a ductile phase itself due to its high slip lines, and it will help improve the ductility of the γ -TiAl alloy. In addition, Schwaighofer et al. [30] proposed that the presence of the γ phases at the colony boundary can intensively retard grain growth, but a high volume fraction of globular γ -grains would lead to a significant decrease of the yield strength at room temperature (RT) and creep strength at elevated temperature. Recently, in our research [31], we concluded that the γ

phase at the α_2/γ colony boundary benefit in terms of improving the ductility of Ti-42Al-5Mn alloy depends on its grain size. This means that the γ phase can only significantly improve the plasticity of the alloy if it has a suitable size, i.e., too large or too small will have more or less adverse effects on the ductility of γ -TiAl alloy plasticity. Hence, it is necessary to effectively control the grain size of the γ phase to ensure that the alloy has good comprehensive performance in the regulation of the alloy microstructure and mechanical properties.

In particular, the fully lamellar microstructure usually exhibits a superior combination of strength, creep resistance, fracture toughness and ductility [32], i.e., the γ phase at α_2/γ colony boundary might be detrimental to the creep strength, then various heat treatments were applied to reduce the volume fraction of γ phase at the α_2/γ colony boundary. For instance, for Ti-44.5Al-6.25Nb-0.8Mo-0.1B (BSG), Bolz et al. [33] found that when treating at 1270 °C, which is just slight below the $T_{\gamma\text{solv}}$ (1280 °C), and finally in combination with a same annealing system (800 °C/6 h/FC), the volume fraction of the globular γ -grain sharply reduced from 61.4% to 12.9% with the increased cooling rate from FC to OC, while that of the lamellar α_2/γ colonies increased intensively from 23.5% to 84.8%. Moreover, they also clarified that the volume fraction of the globular γ -grain can decrease to nearly zero when treating at 1300 °C holding for 1 h and cooling with the AC method, in combination with the 800 °C/6 h/FC annealing system. This means that treating at a higher temperature (normally above $T_{\gamma\text{solv}}$) and combining with a higher cooling rate can help to suppress the globular γ -grain, which inversely promotes γ_1 formation under 800 °C/6 h/FC annealing system. Based on the present research, for Ti-42Al-5Mn, it was also seen that the γ' morphology can gradually transition from globular to platelet, and both γ_g and γ_p can disappear completely with an increased treating temperature above $T_{\gamma\text{solv}}$ combined with a high cooling rate (WQ, OC). Due to the absence of annealing treatment, for the sample accompanied with no γ_g and γ_p phases, large amounts of supersaturated α_2 phase would in turn form.

For the binary TiAl alloys (CG), it should be clarified that the globular γ -grain can emerge when the treating temperature is in the ($\alpha + \gamma$) region. With temperature increases to above $T_{\gamma\text{solv}}$, the full lamellar microstructure without any globular γ -grains can be formed. This suggests that the γ phase at the α_2/γ colony boundary can be completely restrained if treating with a relatively high temperature above $T_{\gamma\text{solv}}$ both for the CG and BSG alloy.

In addition, it should be mentioned that the parent phase of the γ phase α_2/γ colony boundary is not consistent in different γ -TiAl alloys. For the CG alloys, it has been claimed that this γ phase would form in the α -phase when the cooling rate is sufficiently high to suppress the formation of lamellar (α_2/γ) microstructure [34,35]. For BSG alloys, however, this γ phase would only nucleate directly from the β phase [36]. In general, the transformation paths of γ either from β or from α are closely related to the solidification pathway of γ -TiAl alloy. For the CG alloys, the solidification procedure is: $L \rightarrow L + \beta \rightarrow \beta + \alpha$ or $L + \alpha \rightarrow \alpha \rightarrow \alpha + \gamma \rightarrow \alpha_2 + \gamma$. At low temperatures, the β phase will completely transform into the α phase. In this situation, the γ phase can only emerge from α phase. In contrast, for the BSG alloys the solidification pathway is: $L \rightarrow L + \beta \rightarrow \beta \rightarrow \beta + \alpha \rightarrow \beta + \alpha + \gamma \rightarrow \beta_o + \alpha_2 + \gamma$. The ($\beta + \alpha$) phase will turn to ($\beta + \alpha + \gamma$) with decreasing temperature. Based on the present results, the γ phase nucleates directly from the β phase while the α phase transforms into α_2/γ lamella with a γ lath inside. The phase transformation from α_2 -Ti₃Al(D0₁₉) of γ -TiAl(L1₀) not only includes the obvious change of the atom stacking order but also the re-adjustment of the localized chemical composition by long-distance diffusion [37]. This phase transformation is controlled by thermal activation and the reaction rate is relatively slow. In fact, Bolz et al. [33] have concluded that a higher driving force is apparently necessary for $\alpha \rightarrow \alpha_2 + \gamma$ (γ_1) than that of $\beta \rightarrow \gamma$ (γ_g and γ_p). On the contrary, both β_o -TiAl(B₂) [38] and γ -TiAl (L1₀) belong to the cubic structure and have the structure correlation shown in Figure 7. Moreover, the local chemical atom composition of β_o is much closer to the γ phase. Hence, it can be seen that the γ phase is more likely to be precipitated from the β phase with the bcc structure than the α phase with the hcp structure.

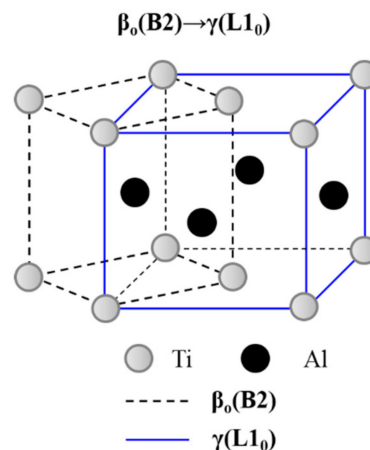


Figure 7. The phase transformation possibility between β_o (B2) and α_2 (L1₀).

5. Conclusions

The phase transformation behavior of Ti-42Al-5Mn alloy from different phase regions with various cooling rates was studied. The basic conclusions are the following:

- I. The $\beta \rightarrow \alpha_2'$ takes place when this alloy is cooled at a high rate (WQ and OC) from β single phase. With the decreasing cooling rate to AC, $\beta \rightarrow \alpha_2'$ is restrained and the $\beta \rightarrow \gamma$ is promoted by the formation of γ platelets.
- II. The room-temperature microstructure is $\beta_o + \alpha_2$ when this alloy is cooled by WQ and OC from ($\beta + \alpha$) the dual-phase. However, under AC, the $\beta \rightarrow \gamma$ takes place and γ platelets form.
- III. The $\alpha_2 \rightarrow \gamma$ occurs when this alloy is cooled from the ($\beta + \alpha + \gamma$) temperature, slightly higher than T_{eut} (1132 °C), by WQ, OC and AC, forming incomplete lamellae (α_2/γ) structures in the α_2 phase. In this situation, plenty of globular γ grains rather than γ platelets are nucleated from the β phase, and the size of γ grains increased intensively with the decreasing cooling rate.
- IV. When the alloy cooled from 1100 °C ($< T_{\text{eut}}$), the $\alpha_2/\gamma \rightarrow \beta_{o,\text{sec}}$ occurs and complete lamellae are generated in the α_2 phase.

Author Contributions: Data curation, X.L. and H.X.; Formal analysis, X.L., W.X. and B.C.; Resources, Y.M.; Supervision, K.L.

Funding: This research was funded by National Natural Science Foundation of China for providing financial support during this study (Project No. 51801210).

Acknowledgments: The authors appreciate Shunnan Zhang at the Institute of Metal Research, Chinese Academy of Sciences, for discussing the microstructural evolution of this alloy. The authors appreciate Yiran Zhou at the center for analysis and testing, Northeastern University.

Conflicts of Interest: The authors declare no conflict of interest.

References

1. Smith, D.; Joris, O.P.; Sankaran, A.; Weekes, H.E.; Bull, D.J.; Prior, T.J.; Dye, D.; Errandonea, D.; Proctor, J.E. On the high-pressure phase stability and elastic properties of β -titanium alloys. *J. Phys. Condens. Matter* **2017**, *29*, 155401. [[CrossRef](#)] [[PubMed](#)]
2. Errandonea, D.; Meng, Y.; Somayazulu, M.; Häusermann, D. Pressure-induced $\alpha \rightarrow \omega$ transition in titanium metal: A systematic study of the effects of uniaxial stress. *Physica B* **2005**, *355*, 116–125. [[CrossRef](#)]
3. Halevy, I.; Zamir, G.; Winterrose, M.; Sanjit, G.; Grandini, C.R.; Moreno-Gobbi, A. Crystallographic structure of Ti-6Al-4V, Ti-HP and Ti-CP under high-pressure. *J. Phys. Conf. Ser.* **2010**, *215*, 1683–1688. [[CrossRef](#)]
4. MacLeod, S.G.; Tegner, B.E.; Cynn, H.; Evans, W.J.; Proctor, J.E.; McMahon, M.I.; Ackland, G.J. Experimental and theoretical study of Ti-6Al-4V to 220 GPa. *Phys. Rev. B* **2012**, *85*, 224202–224207. [[CrossRef](#)]
5. Appel, F.; Wagner, R. Microstructure and deformation of two-phase γ -titanium aluminides. *Mater. Sci. Eng. R Rep.* **1998**, *22*, 187–268. [[CrossRef](#)]

6. Clemens, H.; Kestler, H. Processing and applications of intermetallic γ -TiAl based alloys. *Adv. Eng. Mater.* **2000**, *2*, 551–570. [[CrossRef](#)]
7. Yamaguchi, M.; Inui, H.; Ito, K. High-temperature structural intermetallics. *Acta Mater.* **2000**, *48*, 307–322. [[CrossRef](#)]
8. Li, Y.; Zhou, L.; Lin, J.; Chang, H.; Li, F. Phase transformation behavior and kinetics of high Nb–TiAl alloy during continuous cooling. *J. Alloys Compd.* **2016**, *668*, 22–26. [[CrossRef](#)]
9. Imayev, V.; Oleneva, T.; Imayev, R.; Christ, H.J.; Fecht, H.J. Microstructure and mechanical properties of low and heavy alloyed γ -TiAl + α_2 -Ti₃Al based alloys subjected to different treatments. *Intermetallics* **2012**, *26*, 91–97. [[CrossRef](#)]
10. Naka, S.; Thomas, M.; Sanchez, C.; Khan, T. Development of third generation castable gamma titanium aluminides: Role of solidification paths. In *Structural Intermetallics*; Nathal, M.V., Darolia, R., Liu, C.T., Martin, P.L., Miracle, D.B., Wagner, R., Yamaguchi, M., Eds.; TMS: Warrendale, PA, USA, 1997; pp. 313–322.
11. Kim, Y.W.; Kim, S.L. Advances in gammalloy materials–processes–application technology: Successes, dilemmas, and future. *JOM* **2018**, *70*, 553–560. [[CrossRef](#)]
12. Yang, J.R.; Xiao, B.; Han, P.; Kou, H.C.; Li, J.S. Microstructure evolution in the mushy zone of a β -solidifying TiAl alloy under different cooling processes. *Adv. Eng. Mater.* **2016**, *18*, 1667–1673. [[CrossRef](#)]
13. Kim, Y.W. Intermetallic alloys based on gamma titanium aluminide. *JOM* **1989**, *41*, 24–30. [[CrossRef](#)]
14. Clemens, H.; Mayer, S. Design, processing, microstructure, properties, and applications of advanced intermetallic TiAl alloys. *Adv. Eng. Mater.* **2013**, *15*, 191–215. [[CrossRef](#)]
15. Mayer, S.; Erdely, P.; Fischer, F.D.; Holec, D.; Kasthuber, M.; Klein, T.; Clemens, H. Intermetallic β -solidifying γ -TiAl based alloys—from fundamental research to application. *Adv. Eng. Mater.* **2017**, *19*, 1600735. [[CrossRef](#)]
16. Leitner, T.; Schloffer, M.; Mayer, S.; Eßlinger, J.; Clemens, H.; Pippan, R. Fracture and R-curve behavior of an intermetallic β -stabilized TiAl alloy with different nearly lamellar microstructures. *Intermetallics* **2014**, *53*, 1–9. [[CrossRef](#)]
17. Tetsui, T.; Shindo, K.; Kobayashi, S.; Takeyama, M. A newly developed hot worked TiAl alloy for blades and structural components. *Scr. Mater.* **2002**, *47*, 399–403. [[CrossRef](#)]
18. Tetsui, T.; Shindo, K.; Kaji, S.; Kobayashi, S.; Takeyama, M. Fabrication of TiAl components by means of hot forging and machining. *Intermetallics* **2005**, *13*, 971–978. [[CrossRef](#)]
19. Tetsui, T.; Kobayashi, T.; Harada, H. Achieving high strength and low cost for hot-forged TiAl based alloy containing β phase. *Mater. Sci. Eng. A* **2012**, *552*, 345–352. [[CrossRef](#)]
20. Tetsui, T.; Harada, H. The influence of oxygen concentration and phase composition on the manufacturability and high-temperature strength of Ti-42Al-5Mn (at%) forged alloy. *J. Mater. Process. Technol.* **2013**, *213*, 752–758. [[CrossRef](#)]
21. Xu, H.; Li, W.; Xing, W.; Shu, L.; Ma, Y.C.; Liu, K. Phase transformation behavior in an as-cast Ti-42Al-5Mn alloy after subsequent quenching at different temperatures. *J. Alloys Compd.* **2018**, in press.
22. Xu, H.; Li, X.; Xing, W.; Shu, L.; Ma, Y.; Liu, K. Phase transformation behavior of a Mn containing β -solidifying γ -TiAl alloy during continuous cooling. *Intermetallics* **2018**, *99*, 51–58. [[CrossRef](#)]
23. Hu, D.; Huang, A.J.; Gregoire, A.; Li, X.; Wu, X.; Loretto, M. Determining continuous cooling phase transformation behavior in Ti-46Al-8Nb using Jominy end quenching. *Mater. Sci. Forum* **2005**, *29*, 172–175.
24. Klein, T. Impact of Mo on the ω_0 phase in β -solidifying Ti Al alloys: An experimental and computational approach. *Intermetallics* **2017**, *85*, 26–33. [[CrossRef](#)]
25. Yang, H.W.; Lin, C. Phase transformation and microstructural evolution in Ti-44Al-4Nb-4Zr alloy during heat treatment. *Metall. Mater. Trans. A* **2006**, *37*, 3191–3196. [[CrossRef](#)]
26. Mayer, S.; Petersmann, M.; Fischer, F.D.; Clemens, H.; Waitz, T.; Antretter, T. Experimental and theoretical evidence of displacive martensite in an intermetallic Mo-containing gamma-TiAl based alloy. *Acta Mater.* **2016**, *115*, 242–249. [[CrossRef](#)]
27. Takeyama, M.; Kobayashi, S. Physical metallurgy for wrought gamma titanium aluminides microstructure control through phase transformations. *Intermetallics* **2005**, *13*, 993–999. [[CrossRef](#)]
28. Hu, D.; Jiang, H. Martensite in a TiAl alloy quenched from beta phase field. *Intermetallics* **2015**, *56*, 87–95. [[CrossRef](#)]

29. Schloffer, M.; Rashkova, B.; Schöberl, T.; Schwaighofer, E.; Zhang, Z.; Clemens, H.; Mayer, S. Evolution of the ω phase in a β -stabilized multi-phase TiAl alloy and its effect on hardness. *Acta Mater.* **2014**, *64*, 241–252. [[CrossRef](#)]
30. Schwaighofer, E.; Clemens, H.; Mayer, S.; Lindemann, J.; Klose, J.; Smarsly, W.; Güther, V. Microstructural design and mechanical properties of a cast and heat-treated intermetallic multi-phase γ -TiAl based alloy. *Intermetallics* **2014**, *44*, 128–140. [[CrossRef](#)]
31. Li, X.; Xu, H.; Xing, W.; Shu, L.; Tang, H.; Chen, B.; Ma, Y.; Liu, K. Microstructural evolution and mechanical properties of a forged beta solidified γ -TiAl alloy in different heat treatments. *J. Alloys Compd.* **2018**, in press.
32. Klein, T.; Usategui, L.; Rashkova, B.; Nó, M.L.; San Juan, J.; Clemens, H.; Mayer, S. Mechanical behavior and related microstructural aspects of a nano-lamellar Ti Al alloy at elevated temperatures. *Acta Mater.* **2017**, *128*, 440–450. [[CrossRef](#)]
33. Bolz, S.; Oehring, M.; Lindemann, J.; Pyczak, F.; Paul, J.; Stark, A.; Lippmann, T.; Schröfer, S.; Roth-Fagaraseanu, D.; Schreyer, A.; et al. Microstructure and mechanical properties of a forged β -solidifying γ -Ti Al alloy in different heat treatment conditions. *Intermetallics* **2015**, *58*, 71–83. [[CrossRef](#)]
34. Prasad, U.; Chaturvedi, M.C. Influence of alloying elements on the kinetics of massive transformation in gamma titanium aluminides. *Metall. Mater. Trans. A* **2003**, *34*, 2053–2066. [[CrossRef](#)]
35. Ramanujan, R.V. Phase transformations in gamma based titanium aluminides. *Int. Mater. Rev.* **2000**, *45*, 217–240. [[CrossRef](#)]
36. Cheng, T.T.; Loretto, M.H. The decomposition of the beta phase in Ti-44Al-8Nb and Ti-44Al-4Nb-4Zr-0.2Si alloys. *Acta Mater.* **1998**, *46*, 4801–4819. [[CrossRef](#)]
37. Leyens, C.; Peters, M. *Titanium and Titanium Alloys*; Chemical Industry Press: Beijing, China, 2003; p. 110.
38. Holec, D.; Legut, D.; Isaeva, L.; Souvatzis, P.; Clemens, H.; Mayer, S. Interplay between effect of Mo and chemical disorder on the stability of β/β_0 -TiAl phase. *Intermetallics* **2015**, *61*, 85–90. [[CrossRef](#)]



© 2018 by the authors. Licensee MDPI, Basel, Switzerland. This article is an open access article distributed under the terms and conditions of the Creative Commons Attribution (CC BY) license (<http://creativecommons.org/licenses/by/4.0/>).